Available online at www.sciencedirect.com

ScienceDirect

Nuclear Physics B 932 (2018) 529–539

NUCLEAR PHYSICS B

www.elsevier.com/locate/nuclphysb

# Cavity effects on the Fermi velocity renormalization in a graphene sheet

Wagner P. Pires [a,b,*], Jeferson Danilo L. Silva [c,d], Alessandra N. Braga [e], Van Sérgio Alves [a], Danilo T. Alves [a,f], E.C. Marino [g]

[a] *Faculdade de Física, Universidade Federal do Pará, 66075-110 Belém, Brazil*
[b] *Programa de Ciências Exatas, Universidade Federal do Oeste do Pará, 68040-470 Santarém, Brazil*
[c] *Campus Salinópolis, Universidade Federal do Pará, 68721-000, Salinópolis, Brazil*
[d] *Campus Parauapebas, Universidade Federal Rural da Amazônia, 68515-000 Parauapebas, Brazil*
[e] *Instituto de Estudos Costeiros, Universidade Federal do Pará, 68600-000 Bragança, Brazil*
[f] *Centro de Física, Universidade do Minho, P-4710-057 Braga, Portugal*
[g] *Instituto de Física, Universidade Federal do Rio de Janeiro, 21941-972 Rio de Janeiro, Brazil*

Received 17 January 2018; received in revised form 24 April 2018; accepted 13 May 2018
Available online 17 May 2018
Editor: Hubert Saleur

**Abstract**

Recently, in the literature, it was shown that the logarithmic renormalization of the Fermi velocity in a plane graphene sheet (which, in turn, is related to the Coulombian static potential associated to electrons in the sheet) is inhibited by the presence of a single parallel conducting plate. In the present paper, we investigate the situation of a suspended graphene sheet in a cavity formed by two conducting plates parallel to the sheet. The effect of a cavity on the interaction between electrons in the graphene is not merely the addition of the effects of each plate individually. From this, one can expect that the inhibition of the renormalization of the Fermi velocity generated by a cavity is not a mere addition of the inhibition induced by each single plate. In other words, the simple addition of the result for the inhibition of the renormalization of the Fermi velocity found in the literature for a single plate could not be used to predict the exact behavior of the inhibition for the graphene between two plates. Here, we show that, in fact, this is what happens and calculate how the presence of a cavity formed by two conducting plates parallel to the suspended graphene sheet amplifies, in a non-additive manner, the inhibition of the logarithmic renormalization of

* Corresponding author at: Faculdade de Física, Universidade Federal do Pará, 66075-110 Belém, Brazil.
*E-mail addresses:* wagner.pires@ufopa.edu.br (W.P. Pires), jdanilo@ufpa.br (J.D.L. Silva), alessandrabg@ufpa.br (A.N. Braga), vansergi@ufpa.br (V.S. Alves), danilo@ufpa.br (D.T. Alves), marino@if.ufrj.br (E.C. Marino).

https://doi.org/10.1016/j.nuclphysb.2018.05.010

the Fermi velocity. In the limits of a single plate and no plates, our formulas recover those found in the literature.


## 1. Introduction

In 1993, Marino [1] proposed an effective and complete description in $2+1$ dimensions for electronic systems moving on a plane, but interacting as particles in $3+1$ dimensions,

$$\mathcal{L}_{\rm PQED} = \frac{1}{2}\frac{F_{\mu\nu}F^{\mu\nu}}{(-\Box)^{1/2}} + \mathcal{L}_{\rm D} + j^{\mu}A_{\mu} - \frac{\xi}{2}A_{\mu}\frac{\partial^{\mu}\partial^{\nu}}{(-\Box)^{1/2}}A_{\nu}, \tag{1}$$

where $\Box$ is the d'Alembertian operator, $\mathcal{L}_{\rm D}$ stands for the Dirac's Lagrangian while the last term corresponds to the gauge fixing term. The model given by Eq. (1), denominated pseudo-quantum electrodynamics (PQED), was recently used in the description of several graphene properties [2–7].

From Eq. (1), one obtains the free photon propagator in Euclidean space,

$$\Delta^{(0)}_{\mu\nu}(k) = \frac{1}{2\sqrt{k^2}}\left[\delta_{\mu\nu} - \left(1-\frac{1}{\xi}\right)\frac{k_{\mu}k_{\nu}}{k^2}\right], \tag{2}$$

where $k_{\mu} = (k_0, \mathbf{k})$ and $\mathbf{k} = (k_1, k_2)$. In the nonretarded regime, considering the Feynman gauge ($\xi = 1$), it becomes

$$\Delta^{(0)}_{\mu\nu}(k_0 = 0, |\mathbf{k}|) = \frac{1}{2|\mathbf{k}|}\delta_{0\mu}\delta_{0\nu}, \tag{3}$$

which leads to the Coulombian potential for static charges (instead of the peculiar logarithmic one from QED in $2+1$ dimensions),

$$V(|\mathbf{r}|) = \frac{e}{4\pi}\frac{1}{|\mathbf{r}|}. \tag{4}$$

In this regime, the electron self-energy in a graphene sheet was calculated in Ref. [8] (see also Refs. [9–12]), and the result in one-loop order is

$$\Sigma_0(\mathbf{p}) = -\frac{e^2(\mathbf{p}\cdot\boldsymbol{\gamma})}{16\pi}\ln\frac{\Lambda}{|\mathbf{p}|}, \tag{5}$$

where $e$ is the nonrenormalized coupling constant, $\gamma^{\mu} = (\gamma^0, \boldsymbol{\gamma})$ stands for the Dirac matrices, and $\Lambda$ is an ultraviolet cutoff introduced in the momentum integrals. From Eq. (5), the renormalized Fermi velocity $v_F^R(|\mathbf{p}|)$ with external momentum $p$ reads [8]

$$v_F^R(|\mathbf{p}|) = v_F\left(1 + \frac{\alpha_F}{4}\ln\frac{\Lambda}{|\mathbf{p}|}\right), \tag{6}$$

where $\alpha_F = e^2/(4\pi v_F)$ is the graphene fine structure constant. Experimental results [13] are in good agreement with the theoretical prediction shown in Eq. (6).

The understanding of interaction effects between electrons in graphene is important from theoretical and experimental points of view, since the Fermi velocity is renormalized by these interactions, and it is connected with some transport properties of graphene. For instance, the

optical conductivity in graphene depends on the renormalized Fermi velocity [14]. In addition, the critical coupling constant, which controls the gap opening between the valence and conduction bands and produces a semimetal-insulator transition phase, depends on the renormalization of the Fermi velocity [15]. In this way, the Fermi velocity renormalization can lead to a considerable increase of the critical coupling for dynamical gap generation and charge-density wave formation in the semimetal-insulator transition. This opening of a gap in graphene is another effect in which the renormalization of the Fermi velocity seems to be important [15].

When the environment imposes boundary conditions to the electromagnetic field in $3+1$ dimensions, the dimensional reduction from the usual QED in $3+1$ dimensions to the model given by Eq. (1) ($2+1$ dimensions) incorporates the effects of these boundary conditions, so that the influence of such external conditions is carried into PQED, generating models denominated cavity pseudo-quantum electrodynamics (Cavity PQED) [16]. In the situation where the environment is a single grounded conducting plate, distant $\rho_0$ and parallel to the graphene sheet, an electron with charge $e$ in the graphene sheet interacts not only with another electron in the same sheet, but also with a certain amount of positive charge $-e$ on the surface of the conducting plate induced by the other electron or, in the context of the method of images, with an image point charge $-e$ associated to the other electron. Therefore, the electrostatic potential $V(|\mathbf{r}|)$ in Eq. (4) is replaced by

$$V(|\mathbf{r}|) = \frac{e}{4\pi}\left(\frac{1}{|\mathbf{r}|} - \frac{1}{\sqrt{|\mathbf{r}|^2 + (2\rho_0)^2}}\right). \tag{7}$$

Taking into account Eq. (7), the free photon propagator in Euclidean space in the nonretarded regime is given by

$$\Delta_{00}^{(0)}(\rho_0, |\mathbf{k}|) = \frac{1}{2|\mathbf{k}|}\left[1 - \exp(-2\rho_0|\mathbf{k}|)\right], \tag{8}$$

and the corresponding electron self-energy in the presence of the plate is given by

$$\Sigma(\rho_0, \mathbf{p}) = -\frac{e^2(\mathbf{p}\cdot\boldsymbol{\gamma})}{16\pi}\left[\ln\frac{\Lambda}{|\mathbf{p}|} - F(\rho_0|\mathbf{p}|)\right], \tag{9}$$

where $F(\rho_0|\mathbf{p}|) > 0$ is made explicit in Ref. [16]. Therefore, the renormalized Fermi velocity in the presence of a grounded conducting plate is

$$v_F^R(\rho_0, |\mathbf{p}|) = v_F\left(1 + \frac{\alpha_F}{4}\ln\frac{\Lambda}{|\mathbf{p}|}\right) - v_F\frac{\alpha_F}{4}F(\rho_0|\mathbf{p}|), \tag{10}$$

where the first term in the right-hand side of Eq. (10) is the renormalization of the Fermi velocity shown in Eq. (6) and calculated in Ref. [8], whereas the second term is responsible for the inhibition of the renormalization given by the first term. Comparing the nonretarded electron–electron interaction in a graphene sheet provided by Eq. (4) with that provided by Eq. (7), one sees that the latter is weaker in intensity, which, in turn, is related to the inhibition of the Fermi velocity given by Eq. (10) and calculated in Ref. [16].

In the present paper, we investigate an extension of the model discussed in Ref. [16], by considering a plane graphene sheet inside a cavity formed by two conducting plates parallel to the sheet. We take as basis the PQED [Eq. (1)] to describe the Coulombian interaction between the electrons, but we take into account the modifications induced by the cavity. As discussed in next section, when one considers a cavity, an electron in the graphene sheet interacts not only

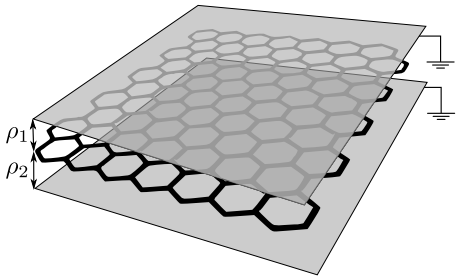


Fig. 1. Illustration of a graphene sheet parallel to two grounded conducting plates, being $\rho_1$ and $\rho_2$ the distances between the graphene sheet and the plates.

with another electron in the sheet, but also with certain amounts of charges on the surfaces of both conducting plates. The distribution of surface charges for the case of a single conducting plate (namely, $-e$) is now affected by the distribution of positive charges on the second plate and vice versa. In the context of the method of images, one can say that, in a cavity, an electron in the graphene sheet interacts not only with another electron in the same sheet, but also with two positive images of this latter and, moreover, with the images of these images, thus interacting with an infinite set of images instead of with a single positive image as it occurs in the case of just one plate. This means that the effect of the presence of a second conducting plate on the interaction between electrons in the graphene sheet is not merely the addition of effects of two single plates. In turn, a priori, the effect of the inhibition of the renormalization of the Fermi velocity produced by the presence of a single plate should be affected by the presence of an other plate and vice versa. Since the mere addition of effects is not expected to be valid, here we calculate how the presence of a cavity amplifies the inhibition of the logarithmic renormalization of the Fermi velocity, if compared to the case of a single plate found in the literature.

The paper is organized as follows. In Sec. 2, we obtain an expression for the photon propagator modified due to the presence of a cavity formed by two grounded perfectly conducting plates. In Sec. 3 we calculate the electron self-energy in one-loop order, and this result is then used to obtain an expression for the renormalized Fermi velocity in a graphene sheet in a cavity. We also discuss the non-additive effects on the renormalized Fermi velocity. In Sec. 4, we present a summary of the results and our final remarks.

## 2. The modified photon propagator

Let us consider an electric charge $e$ in the valence shell of a graphene sheet at distances $\rho_1$ and $\rho_2$ from two grounded and perfectly conducting plates (see Fig. 1). The electrostatic potential vanishes on the plates. Using the method of images, the parallel plates create an infinite set of images symmetrically distributed with respect to the plates, where the first four images are shown in Fig. 2. Let us consider a point $P$ at a distance $|\mathbf{r}|$ from a real charge $e$, both belonging to a line parallel to the plates, as we depict in Fig. 2. The potential $V$, associated with the real charge $e$ and the infinite set of images originated by it, is given by

$$V(|\mathbf{r}|) = \frac{e}{4\pi}\frac{1}{|\mathbf{r}|} + \frac{e}{4\pi}\sum_{n=1}^{\infty}\left[\frac{2}{\sqrt{|\mathbf{r}|^2+4n^2(\rho_1+\rho_2)^2}} - \frac{1}{\sqrt{|\mathbf{r}|^2+4[n\rho_1+(n-1)\rho_2]^2}} - \frac{1}{\sqrt{|\mathbf{r}|^2+4[(n-1)\rho_1+n\rho_2]^2}}\right], \tag{11}$$

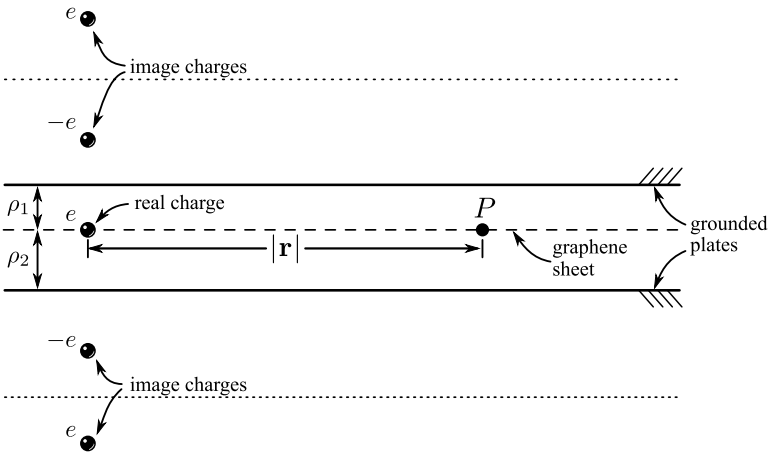


Fig. 2. The first four images of the electron generated by the two grounded plates.

which presents azimuthal symmetry. In this case, when $\rho_1 = \rho_2$ the formula given in Eq. (11) recovers that found in the literature [17] and, in the limit $\rho_1 \to \infty$ (or $\rho_2 \to \infty$), one recovers the potential for just one plate [16]. Let us to write this potential in a more expanded form,

$$V(|\mathbf{r}|) = \frac{e}{4\pi}\frac{1}{|\mathbf{r}|} - \frac{e}{4\pi}\frac{1}{\sqrt{|\mathbf{r}|^2 + (2\rho_1)^2}} - \frac{e}{4\pi}\frac{1}{\sqrt{|\mathbf{r}|^2 + (2\rho_2)^2}} + \frac{e}{4\pi}\frac{2}{\sqrt{|\mathbf{r}|^2 + 4(\rho_1+\rho_2)^2}} + \frac{e}{4\pi}\sum_{n=2}^{\infty}\left[\frac{2}{\sqrt{|\mathbf{r}|^2 + 4n^2(\rho_1+\rho_2)^2}} - \frac{1}{\sqrt{|\mathbf{r}|^2 + 4[n\rho_1 + (n-1)\rho_2]^2}} - \frac{1}{\sqrt{|\mathbf{r}|^2 + 4[(n-1)\rho_1 + n\rho_2]^2}}\right], \tag{12}$$

where one can visualize, on the right-hand side: the first term corresponds to the usual static Coulombian interaction; the second and third terms correspond to the addition of contributions from, respectively, the plates distant $\rho_1$ and $\rho_2$ individually; and the remaining terms reflect the interaction of each plate with the other, breaking the mere addition of effects of single plates.

Using the static potential given by Eq. (11), we can get the "00" component of the photon propagator for electrons constrained to the graphene plane, by means of the inverse Fourier transform, namely (see, for instance, Ref. [18])

$$\Delta_{00}^{(0)}(k_0 = 0, |\mathbf{k}|) = \frac{1}{e^2}\int \mathrm{d}^2\mathbf{r}\, \mathrm{e}^{-i\mathbf{k}\cdot\mathbf{r}} e V(|\mathbf{r}|), \tag{13}$$

with $\mathbf{k}$ and $\mathbf{r}$ being restricted to the graphene plane, so that $\mathrm{d}^2\mathbf{r} = |\mathbf{r}|\,\mathrm{d}|\mathbf{r}|\,\mathrm{d}\varphi$, $\mathbf{k}\cdot\mathbf{r} = |\mathbf{k}|\,|\mathbf{r}|\cos\varphi$, where $\varphi$ is integrated from 0 to $2\pi$ and $|\mathbf{r}|$ from 0 to infinity. Therefore we get, in a similar way as done in Ref. [16],

$$\Delta_{00}^{(0)}(\rho_1, \rho_2, |\mathbf{k}|) = \frac{1}{2|\mathbf{k}|}\left[1 + \left(2 - \mathrm{e}^{2|\mathbf{k}|\rho_1} - \mathrm{e}^{2|\mathbf{k}|\rho_2}\right)\sum_{n=1}^{\infty}\mathrm{e}^{-2|\mathbf{k}|n(\rho_1+\rho_2)}\right]. \tag{14}$$

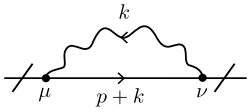


Fig. 3. One-loop electron self-energy diagram.

The sum in (14) is a simple geometric sequence. Solving this we have

$$\Delta_{00}^{(0)}(\rho_1,\rho_2,|\mathbf{k}|)=\frac{1}{2|\mathbf{k}|}\left(1+\frac{2\mathrm{e}^{-2|\mathbf{k}|(\rho_1+\rho_2)}-\mathrm{e}^{-2|\mathbf{k}|\rho_1}-\mathrm{e}^{-2|\mathbf{k}|\rho_2}}{1-\mathrm{e}^{-2|\mathbf{k}|(\rho_1+\rho_2)}}\right). \tag{15}$$

The first term in the right-hand side of Eq. (15) is the free propagator and the second one arises due to the presence of the plates. Next, we shall use the modified propagator (15) to obtain a new expression for the electron self-energy, from which we will get the renormalized Fermi velocity in the presence of the cavity.

## 3. Electron self-energy, renormalized Fermi velocity and non-additive effects

The Dirac's Lagrangian that describes the massless electrons moving with a Fermi velocity in the graphene valence shell is given by

$$\mathcal{L}_{\mathrm{D}}=\bar{\psi}_a\left(i\gamma^0\partial_0+iv_F\boldsymbol{\gamma}\cdot\nabla\right)\psi_a, \tag{16}$$

where $\bar{\psi}_a=\psi_a^\dagger\gamma^0$, $a$ is a flavor index representing a sum over valleys $K$ and $K'$, $\gamma^\mu$ are rank-4 Dirac matrices and $\psi_a^\dagger=\left(\psi_{A\uparrow}^\star\ \psi_{A\downarrow}^\star\ \psi_{B\uparrow}^\star\ \psi_{B\downarrow}^\star\right)_a$ a four-component Dirac spinor representing electrons in sublattices $A$ and $B$ in graphene, with different spin orientations.

Using the Lagrangian (16), we obtain the following bare fermion propagator

$$S_F^{(0)}(k^\mu)=\frac{k_0\gamma^0+v_F\mathbf{k}\cdot\boldsymbol{\gamma}}{k_0^2+v_F^2|\mathbf{k}|^2}. \tag{17}$$

If we consider only the static case ($v_F/c\ll 1$), which means that the vertex interaction is $e\gamma^0$, the one-loop electron self-energy (see Fig. 3) reads (since this calculation does not involve a fermion loop, it is sufficient to consider only one species of fermions)

$$\Sigma(\rho_1,\rho_2,\mathbf{p})=e^2\int\frac{\mathrm{d}^2\mathbf{k}}{(2\pi)^2}\frac{\mathrm{d}k_0}{2\pi}\gamma^0S_F^{(0)}(k^\mu+p^\mu)\gamma^0\Delta_{00}^{(0)}(\rho_1,\rho_2,|\mathbf{k}|), \tag{18}$$

which can be rewritten as

$$\Sigma(\rho_1,\rho_2,\mathbf{p})=\Sigma_0(\mathbf{p})+\tilde{\Sigma}(\rho_1,\rho_2,\mathbf{p}), \tag{19}$$

where $\Sigma_0$ is the self-energy in the absence of the plate (recovered when $\rho_1\to\infty$ and $\rho_2\to\infty$), and $\tilde{\Sigma}$ is the contribution due to the presence of the cavity, namely

$$\Sigma_0(\mathbf{p})=-\frac{e^2}{2}\int\frac{\mathrm{d}^2\mathbf{k}}{(2\pi)^2}\frac{(\mathbf{k}+\mathbf{p})\cdot\boldsymbol{\gamma}}{|\mathbf{k}+\mathbf{p}|}\frac{1}{2|\mathbf{k}|}, \tag{20}$$

$$\tilde{\Sigma}(\rho_1,\rho_2,\mathbf{p})=-\frac{e^2}{2}\int\frac{\mathrm{d}^2\mathbf{k}}{(2\pi)^2}\frac{(\mathbf{k}+\mathbf{p})\cdot\boldsymbol{\gamma}}{|\mathbf{k}+\mathbf{p}|}\frac{1}{2|\mathbf{k}|}\left(\frac{2\mathrm{e}^{-2|\mathbf{k}|(\rho_1+\rho_2)}-\mathrm{e}^{-2|\mathbf{k}|\rho_1}-\mathrm{e}^{-2|\mathbf{k}|\rho_2}}{1-\mathrm{e}^{-2|\mathbf{k}|(\rho_1+\rho_2)}}\right). \tag{21}$$

With the same procedure shown in [9,16], where it is used elliptical coordinates and regularization by cutoff, Eq. (21) can be written as

$$\tilde{\Sigma}(\rho_1, \rho_2, |\mathbf{p}|) = -\frac{(\mathbf{p}\cdot\boldsymbol{\gamma})e^2}{16\pi^2}\left[L_1(\rho_1|\mathbf{p}|, \rho_2|\mathbf{p}|) + L_2(\rho_1|\mathbf{p}|, \rho_2|\mathbf{p}|)\right], \tag{22}$$

where

$$L_1(\rho_1|\mathbf{p}|, \rho_2|\mathbf{p}|) = \int_0^{2\pi} \mathrm{d}\nu \int_0^{\mu_\Lambda} \mathrm{d}\mu\ f(\rho_1|\mathbf{p}|, \rho_2|\mathbf{p}|; \mu, \nu), \qquad \mu_\Lambda = \cosh^{-1}(2\Lambda/|\mathbf{p}| + \cos\nu), \tag{23}$$

$$L_2(\rho_1|\mathbf{p}|, \rho_2|\mathbf{p}|) = \int_0^{2\pi} \mathrm{d}\nu \cos\nu \int_0^{\mu_\Lambda} \mathrm{d}\mu \cosh\mu\ f(\rho_1|\mathbf{p}|, \rho_2|\mathbf{p}|; \mu, \nu), \tag{24}$$

and

$$f(\rho_1|\mathbf{p}|, \rho_2|\mathbf{p}|; \mu, \nu) = \frac{1}{2\pi}\left[\frac{2\mathrm{e}^{-|\mathbf{p}|(\rho_1+\rho_2)(\cosh\mu-\cos\nu)} - \mathrm{e}^{-\rho_1|\mathbf{p}|(\cosh\mu-\cos\nu)} - \mathrm{e}^{-\rho_2|\mathbf{p}|(\cosh\mu-\cos\nu)}}{1-\mathrm{e}^{-|\mathbf{p}|(\rho_1+\rho_2)(\cosh\mu-\cos\nu)}}\right]. \tag{25}$$

Therefore, using (22) and the free electron self-energy that arises from (20), the complete electron self-energy in the cavity (19) can be written as

$$\Sigma(\rho_1, \rho_2, |\mathbf{p}|) = -\frac{e^2(\mathbf{p}\cdot\boldsymbol{\gamma})}{16\pi}\left[\ln\frac{\Lambda}{|\mathbf{p}|} + L_1(\rho_1|\mathbf{p}|, \rho_2|\mathbf{p}|) + L_2(\rho_1|\mathbf{p}|, \rho_2|\mathbf{p}|)\right]. \tag{26}$$

Since the complete fermion propagator is given by

$$S_F^{-1}(p^\mu) = -p_\mu\gamma^\mu + \Sigma(p^\mu) = -p_0\gamma^0 - v_F(\mathbf{p}\cdot\boldsymbol{\gamma}) + \Sigma(p^\mu), \tag{27}$$

from (26), we identify the renormalized Fermi velocity inside a grounded conducting cavity as

$$\frac{v_F^R(\rho_1, \rho_2, |\mathbf{p}|)}{v_F} = 1 + \frac{\alpha_F}{4}\left[\ln\frac{\Lambda}{|\mathbf{p}|} + L_1(\rho_1|\mathbf{p}|, \rho_2|\mathbf{p}|) + L_2(\rho_1|\mathbf{p}|, \rho_2|\mathbf{p}|)\right], \tag{28}$$

where $L_1$ and $L_2$ are given by (23) and (24) respectively. The dependence of (28) in terms of $\rho_1$, $\rho_2$ and $|\mathbf{p}|$ can be analyzed numerically.

In Fig. 4, we show the renormalized Fermi velocity for some values of $\rho_1$ and $\rho_2$. The solid (blue) line is the renormalization without plates, as found in Ref. [8]. When we bring a single conducting plate near the graphene sheet, we have an inhibition of the renormalization, as shown by the dashed (red) and dot-dashed (orange) lines, for $\rho_1 = 100/\Lambda$ and $\rho_1 = 10/\Lambda$, respectively, as found in Ref. [16]. If a second conducting plate is put together, for instance at the same distance of the first one ($\rho_1 = \rho_2$), we have an amplification of the inhibition, as shown by the dotted (green) and long-dashed (purple) lines, for $\rho_1 = \rho_2 = 100/\Lambda$ and $\rho_1 = \rho_2 = 10/\Lambda$, respectively. As $|\mathbf{p}|$ grows, the amplification caused by the second plate diminishes, so that two plates tend to act as a single plate [for instance, the dotted (green) line converges to the dashed (red) line]. Moreover, as $|\mathbf{p}|$ grows, the inhibition caused by plates tends to disappear, so that one recovers the renormalization without plates [for example, the dashed (red) and dotted (green) lines converge to the solid (blue) line].

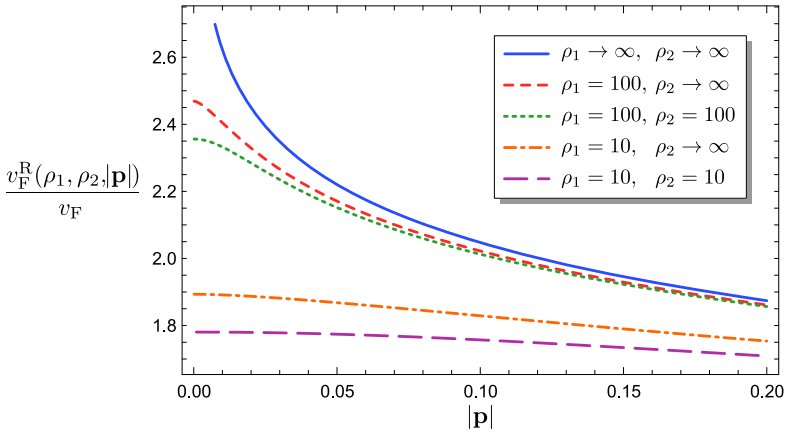


Fig. 4. (Color online) Renormalized Fermi velocity as a function of the external momentum $|\mathbf{p}|$, for several values of $\rho_1$ and $\rho_2$ (considering $\Lambda = \alpha_F = 1$).

The non-additivity in the amplification of the inhibition of the renormalization of the Fermi velocity can be investigated as follows. Let us consider the expansion

$$\left[1 - \mathrm{e}^{-|\mathbf{p}|(\rho_1+\rho_2)(\cosh\mu-\cos\nu)}\right]^{-1} = \sum_{n=0}^{\infty} \mathrm{e}^{-n|\mathbf{p}|(\rho_1+\rho_2)(\cosh\mu-\cos\nu)}, \tag{29}$$

from which we rewrite the Eq. (25) as

$$f(\rho_1|\mathbf{p}|,\rho_2|\mathbf{p}|;\mu,\nu) = f(\rho_1|\mathbf{p}|,\infty;\mu,\nu) + f(\infty,\rho_2|\mathbf{p}|;\mu,\nu) + f_{\mathrm{cross}}(\rho_1|\mathbf{p}|,\rho_2|\mathbf{p}|;\mu,\nu), \tag{30}$$

where $f(\rho_1|\mathbf{p}|,\infty;\mu,\nu)$ and $f(\infty,\rho_2|\mathbf{p}|;\mu,\nu)$ directly come from the Eq. (25), and

$$\begin{aligned} &f_{\mathrm{cross}}(\rho_1|\mathbf{p}|,\rho_2|\mathbf{p}|;\mu,\nu) \\ &= \frac{1}{2\pi}\left[2\mathrm{e}^{-|\mathbf{p}|(\rho_1+\rho_2)(\cosh\mu-\cos\nu)} - \mathrm{e}^{-\rho_1|\mathbf{p}|(\cosh\mu-\cos\nu)} - \mathrm{e}^{-\rho_2|\mathbf{p}|(\cosh\mu-\cos\nu)}\right] \\ &\quad\times \sum_{n=1}^{\infty} \mathrm{e}^{-n|\mathbf{p}|(\rho_1+\rho_2)(\cosh\mu-\cos\nu)} + \frac{1}{\pi}\mathrm{e}^{-|\mathbf{p}|(\rho_1+\rho_2)(\cosh\mu-\cos\nu)}. \end{aligned} \tag{31}$$

In Eq. (30) one can visualize, on the right-hand side, the first and second terms corresponding to the contributions from, respectively, the plates distant $\rho_1$ and $\rho_2$ separately, whereas the remaining term, $f_{\mathrm{cross}}$, depends on $\rho_1$ and $\rho_2$ simultaneously, reflecting the effect of the interaction of each plate with the other. Using Eqs. (30) and (31) in (23) and (24), we can rewrite Eq. (28) as

$$\frac{v_F^R(\rho_1,\rho_2,|\mathbf{p}|)}{v_F} = 1 + \frac{\alpha_F}{4}\ln\frac{\Lambda}{|\mathbf{p}|} + \frac{\alpha_F}{4}L_{\mathrm{plates}}(\rho_1|\mathbf{p}|,\rho_2|\mathbf{p}|) + \frac{\alpha_F}{4}L_{\mathrm{cross}}(\rho_1|\mathbf{p}|,\rho_2|\mathbf{p}|), \tag{32}$$

with

$$L_{\mathrm{plates}}(\rho_1|\mathbf{p}|,\rho_2|\mathbf{p}|) = L_1(\rho_1|\mathbf{p}|,\infty) + L_2(\rho_1|\mathbf{p}|,\infty) + L_1(\infty,\rho_2|\mathbf{p}|) + L_2(\infty,\rho_2|\mathbf{p}|) \tag{33}$$

and

$$L_{\mathrm{cross}}(\rho_1|\mathbf{p}|,\rho_2|\mathbf{p}|) = L_{1\mathrm{cross}}(\rho_1|\mathbf{p}|,\rho_2|\mathbf{p}|) + L_{2\mathrm{cross}}(\rho_1|\mathbf{p}|,\rho_2|\mathbf{p}|), \tag{34}$$

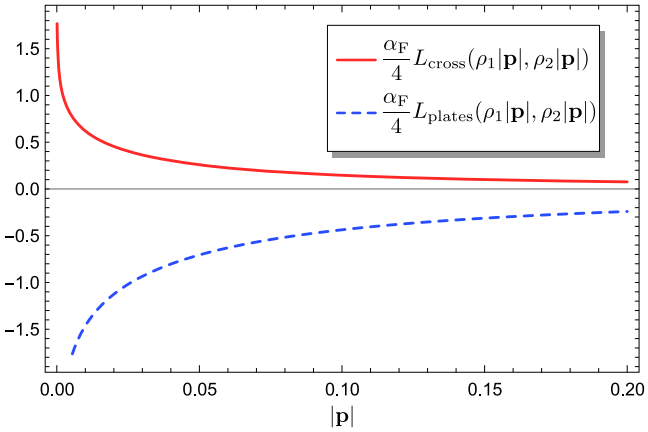


Fig. 5. (Color online) Comparison between $(\alpha_F/4)L_{\text{plates}}$ [dashed (blue) line] and $(\alpha_F/4)L_{\text{cross}}$ [solid (red) line], for $\rho_1 = \rho_2 = 10$, and considering $\Lambda = \alpha_F = 1$.

where $L_{1\text{cross}}(\rho_1|\mathbf{p}|, \rho_2|\mathbf{p}|)$ and $L_{2\text{cross}}(\rho_1|\mathbf{p}|, \rho_2|\mathbf{p}|)$ are obtained by replacement of $f$ by $f_{\text{cross}}$ in Eqs. (23) and (24). On the right-hand side of Eq. (32), the first and second terms correspond to the renormalization of the Fermi velocity found in Ref. [8]. The third term, involving $L_{\text{plates}}(\rho_1|\mathbf{p}|, \rho_2|\mathbf{p}|)$, is the addition of the contribution of each plate individually. The fourth term, involving $L_{\text{cross}}(\rho_1|\mathbf{p}|, \rho_2|\mathbf{p}|)$, depends on $\rho_1$ and $\rho_2$ simultaneously and is responsible for the non-additive effects.

In Fig. 5, we compare the contribution from the term involving $L_{\text{plates}}$ with that coming from the term involving $L_{\text{cross}}$. We can see that the contribution from the $L_{\text{plates}}$ term [shown by the dashed (blue) line] is negative, which means that this term inhibits the renormalization of the Fermi velocity. On the other hand, the contribution from the $L_{\text{cross}}$ term [shown by the solid (red) line] is positive, contributing to an enhancement of the renormalization. Once the magnitude of the $L_{\text{plates}}$ term is greater than the magnitude of the $L_{\text{cross}}$ term, the net effect is still an inhibition of the renormalization of the Fermi velocity, but now amplified if compared to the case of a single plate. This result can be understood as follows. The contribution from the $L_{\text{plates}}$ term comes from the first two image charges, both with charge $-e$, shown in Fig. 2. These positive image charges generate an electric field at the point $P$, whose component parallel to the graphene sheet has direction opposite to the electric field generated by the real negative charge $e$, reducing the magnitude of the effective static potential associated to $e$. This, in turn, tends to diminish the renormalization of the Fermi velocity. However, the complete impact of the conducting plates on the renormalization requires to compute the effect of the other infinity image charges, which are, in fact, images of images, reflecting the interaction of each plate with the other, which is responsible for the non-additive effect. For instance, let us consider the effect of the other two image charges, both with charge $e$, shown in Fig. 2. The component parallel to the graphene sheet of the electric field at the point $P$, generated by these negative image charges, has the same direction of the electric field generated by the real charge $e$, which tends to enhance the magnitude of the effective static potential associated to $e$ and, as a consequence, tends to enhance the renormalization of the Fermi velocity. Since the two negative image charges $e$ shown in Fig. 2 are more distant from $P$ than the positive image charges $-e$, the inhibition effect caused by the latter charges predominates. Taking into account all image charges beyond those shown in Fig. 2, we get $L_{\text{cross}} > 0$ and $|L_{\text{cross}}| < |L_{\text{plates}}|$. Then, the net effect of the infinity image charges or, in

other words, of the induced charges on the conducting plates, is a reduction of the magnitude of the effective static potential associated to $e$, which means inhibition of the renormalization of the Fermi velocity.

## 4. Final remarks

We showed how the inhibition of the renormalization of the Fermi velocity behaves when we bring two grounded perfectly conducting plates near a suspended graphene sheet [Eq. (32)]. In this case, the inhibition is amplified in comparison to the case of a single plate found in the literature, but it is not a mere addition of the inhibition induced by each single plate separately. In fact, the pure additive sector, stored in $L_{\text{plates}}$ [Eq. (33)], is just a part of the complete renormalization formula given by Eq. (32). Breaking the pure additivity, we obtained the term $L_{\text{cross}}$ [Eq. (34)], which stores the effects of the interaction between the induced charges in a plate with the other plate and vice versa. It was shown that $L_{\text{plates}} < 0$, which means that it contributes to inhibit the renormalization of the Fermi velocity, whereas $L_{\text{cross}} > 0$ contributes to an enhancement of the renormalization. Since $|L_{\text{cross}}| < |L_{\text{plates}}|$, the inhibition (now amplified) predominates.

In the limit of no plates, the formula presented here [Eq. (32)] recovers the Eq. (6), which was obtained in Ref. [8] and it is in good agreement with experimental results [13]. Our results shown in Eq. (32) may have consequences in some transport properties of graphene since, for instance, according to Eq. (5) found in Ref. [14], the difference between the optical conductivity and the universal conductivity in graphene depends inversely on the renormalized Fermi velocity. Therefore the inhibition of the renormalized Fermi velocity leads to an increase of the optical conductivity. In this context, an experimental verification of the inhibition of the renormalized Fermi velocity by the presence of a single conducting plate, or the inhibition amplified by the presence of a second plate (cavity), seems feasible. In addition, if an experimental measurement of the inhibition of the Fermi velocity renormalization in the presence of a cavity considers a sufficient low density of states (small external momentum) and small distances between the plates, then the crossed term [Eq. (34)] is an important part of the total inhibition, as shown in Figs. 4 and 5. In this way, although the crossed term is exponentially suppressed with the distance between the plates, depending on the experimental set up it could be relevant.

It is appropriate to emphasize that the Eq. (6) [8] is only valid in the regime where $v_F \ll c$. In the retarded regime where $v_F \approx c$, the renormalization of the Fermi velocity is power-law instead of logarithmic [8,19]. The effects of conducting plates on the renormalization of the Fermi velocity in the retarded regime, as well as more realistic models of Cavity PQED, are under investigation.

## Acknowledgements

This work was partially supported by the following Brazilian Agencies: Coordenação de Aperfeiçoamento de Pessoal de Nível Superior (CAPES), Conselho Nacional de Desenvolvimento Científico e Tecnológico (CNPq), and Fundação de Amparo à Pesquisa do Estado do Rio de Janeiro (FAPERJ). E. C. Marino was partially supported by CNPq and FAPERJ. D. T. Alves was partially supported by CAPES via Programa Estágio Sênior no Exterior – Processo 88881.119705/2016-01, by CNPq via Processos 461826/2014-3 (Edital Universal) and 311920/2014-4 (Bolsa de Produtividade em Pesquisa), and also thanks Jaime Santos, Mikhail I. Vasilevskiy, Nuno M. R. Peres and Yuliy Bludov for useful discussions, as well as the hospitality of the Centro de Física, Universidade do Minho, Braga – Portugal. V. S. Alves acknowledges

CNPq for support through Bolsa de Produtividade em Pesquisa n. 312654/2017-0. The authors also thank Ygor P. Silva for useful comments.

## References

[1] E.C. Marino, Quantum electrodynamics of particles on a plane and the Chern–Simons theory, Nucl. Phys. B 408 (1993) 551, https://doi.org/10.1016/0550-3213(93)90379-4.
[2] V.S. Alves, W.S. Elias, L.O. Nascimento, V. Juričić, F. Peña, Chiral symmetry breaking in the pseudo-quantum electrodynamics, Phys. Rev. D 87 (2013) 125002, https://doi.org/10.1103/PhysRevD.87.125002.
[3] L.O. Nascimento, V.S. Alves, F. Peña, C.M. Smith, E.C. Marino, Chiral-symmetry breaking in pseudoquantum electrodynamics at finite temperature, Phys. Rev. D 92 (2015) 025018, https://doi.org/10.1103/PhysRevD.92.025018.
[4] E.C. Marino, L.O. Nascimento, V.S. Alves, C.M. Smith, Interaction induced quantum valley Hall effect in graphene, Phys. Rev. X 5 (2015) 011040, https://doi.org/10.1103/PhysRevX.5.011040.
[5] N. Menezes, V.S. Alves, C.M. Smith, The influence of a weak magnetic field in the renormalization-group functions of $(2+1)$-dimensional Dirac systems, Eur. Phys. J. B 89 (12) (2016) 271, https://doi.org/10.1140/epjb/e2016-70606-4.
[6] V.S. Alves, R.O.C. Junior, E.C. Marino, L.O. Nascimento, Dynamical mass generation in pseudoquantum electrodynamics with four-fermion interactions, Phys. Rev. D 96 (2017) 034005, https://doi.org/10.1103/PhysRevD.96.034005.
[7] N. Menezes, V.S. Alves, E.C. Marino, L. Nascimento, L.O. Nascimento, C. Morais Smith, Spin $g$-factor due to electronic interactions in graphene, Phys. Rev. B 95 (2017) 245138, https://doi.org/10.1103/PhysRevB.95.245138.
[8] J. González, F. Guinea, M.A.H. Vozmediano, Non-Fermi liquid behavior of electrons in the half-filled honeycomb lattice (A renormalization group approach), Nucl. Phys. B 424 (1994) 595, https://doi.org/10.1016/0550-3213(94)90410-3.
[9] E. Barnes, E.H. Hwang, R.E. Throckmorton, S. Das Sarma, Effective field theory, three-loop perturbative expansion, and their experimental implications in graphene many-body effects, Phys. Rev. B 89 (2014) 235431, https://doi.org/10.1103/PhysRevB.89.235431.
[10] A.H. Castro Neto, F. Guinea, N.M.R. Peres, K.S. Novoselov, A.K. Geim, The electronic properties of graphene, Rev. Mod. Phys. 81 (2009) 109, https://doi.org/10.1103/RevModPhys.81.109.
[11] M.A.H. Vozmediano, Renormalization group aspects of graphene, Philos. Trans. R. Soc. Lond. Ser. A 369 (2011) 2625, https://doi.org/10.1098/rsta.2010.0383.
[12] M.A.H. Vozmediano, F. Guinea, Effect of Coulomb interactions on the physical observables of graphene, Phys. Scr. 2012 (2012) 014015, https://doi.org/10.1088/0031-8949/2012/T146/014015.
[13] D.C. Elias, R.V. Gorbachev, A.S. Mayorov, S.V. Morozov, A.A. Zhukov, P. Blake, L.A. Ponomarenko, I.V. Grigorieva, K.S. Novoselov, F. Guinea, A.K. Geim, Dirac cones reshaped by interaction effects in suspended graphene, Nat. Phys. 7 (2011) 701, https://doi.org/10.1038/nphys2049.
[14] T. Stauber, P. Parida, M. Trushin, M.V. Ulybyshev, D.L. Boyda, J. Schliemann, Interacting electrons in graphene: Fermi velocity renormalization and optical response, Phys. Rev. Lett. 118 (2017) 266801, https://doi.org/10.1103/PhysRevLett.118.266801.
[15] C. Popovici, C.S. Fischer, L. von Smekal, Fermi velocity renormalization and dynamical gap generation in graphene, Phys. Rev. B 88 (2013) 205429, https://doi.org/10.1103/PhysRevB.88.205429.
[16] J.D.L. Silva, A.N. Braga, W.P. Pires, V.S. Alves, D.T. Alves, E.C. Marino, Inhibition of the Fermi velocity renormalization in a graphene sheet by the presence of a conducting plate, Nucl. Phys. B 920 (2017) 221, https://doi.org/10.1016/j.nuclphysb.2017.04.014.
[17] J. Pumplin, Application of Sommerfeld–Watson transformation to an electrostatics problem, Am. J. Phys. 37 (7) (1969) 737, https://doi.org/10.1119/1.1975793.
[18] C.D. Roberts, A.G. Williams, Dyson–Schwinger equations and their application to hadronic physics, Prog. Part. Nucl. Phys. 33 (1994) 477, https://doi.org/10.1016/0146-6410(94)90049-3.
[19] E.C. Marino, Quantum Field Theory Approach to Condensed Matter Physics, Cambridge University Press, Cambridge and New York, 2017.